CHAPTER 3

Methodology

In this chapter, the following topics will be discussed:

- Observations at the Thai National Observatory (TNO) during six nights in February - March, 2014 with multi-bandpass optical observations,
- Raw image data reduction pipeline via IRAF (Image Reduction and Analysis Facility), and
- The "Aperture Photometry", including the determination of the star's magnitude, the galaxies' magnitude and its boundaries, zero-points, and filter corrections via Starlink, an astronomical data processing program, run on UNIX's environment system, that analyzes the photometry imaging data.

3.1 The Observations

3.1.1 The Target of the Study

In this research, I focus on the compact group of galaxy called NGC 4065. The center of the group is located at right ascension (RA), 12h 04m 0.95s, and declination (DEC), +20° 13' 18.00", observable at the northern hemisphere including Thailand. Using the Simbad Astronomical Database and NASA/IPAC Extragalactic Database (NED), we have resolved the average radial velocity of this group which is equal to 7045 km/s or redshift of 0.0235. From the redshift information, the distance from the Earth to the group, equal to 105.1 ± 1.8 Mpc, can be calculated using Eq. 3.1.

$$d = \frac{v}{H_0} = \frac{z \cdot c}{H_0} \quad , \tag{3.1}$$

where

d is the distance,

v is the radial velocity,

H_0 is the Hubble constant (67.6 ± 1.2 km.s^{-1}Mpc^{-1}),

z is the redshift of the object, and

c is the speed of light.

3.1.2 Observing Instrument

The imaging data was taken using the 2.4 meter Ritchey-Chretien Alt-Azimuth Drive Reflecting telescope at the Thai National Observatory (TNO) connected to a 2048x2048 pixel Apogee-U42 CCD (4'x4' field of view, FOV), located at Doi Inthanon, Chiang Mai, Thailand, which is 2,457 meters above the mean sea level, last 25 - 27 February and 9 - 11 March 2014 with ten observation points as shown in Figure 3.1. Each observation point was taken five times using different filters and exposure times, 900 s, 600 s and 300 s for BVR_C Johnson-Cousins's broadband filters, respectively, and 900 s for both [SII] and Red-continuum narrowband filters. The exposure time was selected by considering throughput efficiency of the filters, maintaining an unsaturated signal value.

This study aims to use BVR_C broadband filters for creating color-color, color-magnitude diagrams. Finding these correlations will help us understand the morphology and nature of our sample galaxies, and use them as criteria for selecting the sample in our work.

[SII] and Red-continuum narrowband filters are used to determine the $EW(\mathrm{H}\alpha)$, which is an indicator of the star formation activity in galaxies [Kennicutt, 1983; Gavazzi et al., 2006; Kriwattanawong et al., 2011]. At our distance, the observational wavelength of Hα emission line is shifted from 656.3 nm to 671.7 nm, which is allowed to transmit in a [SII] narrowband filter. Thus, we chose the [SII] narrowband filter to obtain the Hα emission line.

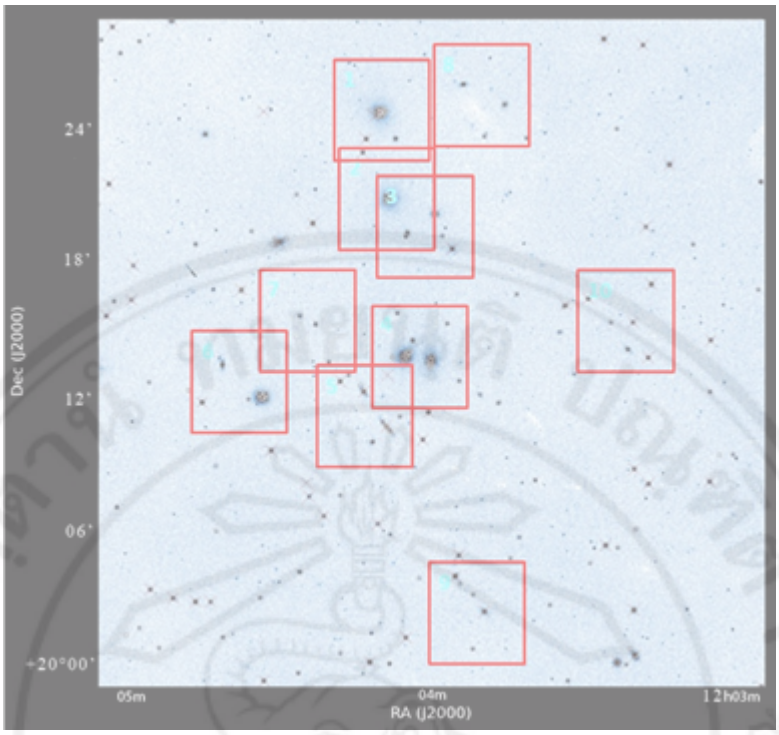

Figure 3.1: The area of NGC 4065 group (30'x30' FOV) overlaid with our ten observation points (4'x4' FOV) which is shown in red boxes with pointer number on top left.

3.1.3 The List of The Sample Data

From the ten imaging data points, I separated the member of the group from background and foreground galaxies using the redshift collected from the NASA/IPAC Extragalactic Database (NED) and SIMBAD Astronomical Database. 21 galaxies were confirmed to be members in the NGC 4065 galaxy group as shown in Table 3.3.

3.2 Image Reduction Pipeline

The raw imaging data contains all the signal read out by the CCD, including the sky image and instrument signatures. Analyzing the raw imaging data directly is not a good idea because the result could be biased by various noise, such as the dark current, the field curvature from the CCD itself, and the unwanted signals from the sky like atmospheric condition, cosmic ray, and sky background. The raw image reduction aims to remove these effects. In this study, we use the Image Reduction and Analysis Facility (IRAF) and

Table 3.1: The sample of galaxies in NGC 4065 group with position and redshift

No.	Name	RA (J2000)	DEC (J2000)	Redshift
1	NGC 4070	12h 04m 11.298s	+20° 24’ 35.11’’	0.0240
2	2MASX J12040831+2023280	12h 04m 08.313s	+20° 23’ 28.09’’	0.0222
3	NGC 4066	12h 04m 09.386s	+20° 20’ 52.10’’	0.0245
4	NGC 4069	12h 04m 06.031s	+20° 19’ 25.96’’	0.0255
5	NGC 4060	12h 04m 00.981s	+20° 20’ 14.97’’	0.0226
6	NGC 4056	12h 03m 57.711s	+20° 18’ 44.98’’	0.0246
7	NGC 4065	12h 04m 06.167s	+20° 14’ 05.95’’	0.0211
8	2MASX J12040495+2014489	12h 04m 04.958s	+20° 14’ 48.96’’	0.0223
9	NGC 4061 (4055)	12h 04m 01.406s	+20° 13’ 55.97’’	0.0240
10	NGC 4072	12h 04m 13.806s	+20° 12’ 35.12’’	0.0217
11	UGC 07049	12h 04m 09.547s	+20° 11’ 05.09’’	0.0251
12	2MASX J12041217+2010251	12h 04m 12.152s	+20° 10’ 24.83’’	0.0214
13	RASSCALS NRGb177.059	12h 04m 40.430s	+20° 13’ 58.16’’	0.0206
14	2MASX J12043987+2013411	12h 04m 39.830s	+20° 13’ 40.90’’	0.0239
15	NGC 4076	12h 04m 32.490s	+20° 12’ 18.14’’	0.0207
16	SDSS J120425.68+201548.9	12h 04m 25.700s	+20° 15’ 49.00’’	0.0237
17	2MASX J12042275+2015271	12h 04m 22.800s	+20° 15’ 27.00’’	0.0213
18	2MASX J12035600+2025499	12h 03m 56.008s	+20° 25’ 49.98’’	0.0219
19	2MASX J12034825+2024589	12h 03m 48.252s	+20° 24’ 58.97’’	0.0212
20	2MASX J12035132+2003099	12h 03m 51.321s	+20° 03’ 09.98’’	0.0222
21	2MASX J12032530+2014294	12h 03m 25.300s	+20° 14’ 29.00’’	0.0193

Starlink package to make the image reduction pipeline.

The imaging data is stored as Flexible Image Transport System (FITS) format that is supported by most astronomical software. From the observation, we have 50 scientific frames (10 frames for each filter), 33 dark frames (11 frames for different exposure times) and 55 flat frames (11 frames for each filter). The dark frames and flat frames were taken as same as the observation night.

3.2.1 Combining the Dark Frames

The dark frame is an image captured with the shutter closed and with the same exposure time as the scientific frame. The aim of the dark frame is to measure the dark current on the CCD caused by electrons generated by the device itself. To combine the dark frames, I used the “darkcombine” task in IRAF using the parameters shown in Figure

3.2 After this task, one master dark frame is obtained, which is the median value of all the dark frames (see Figure 3.3).

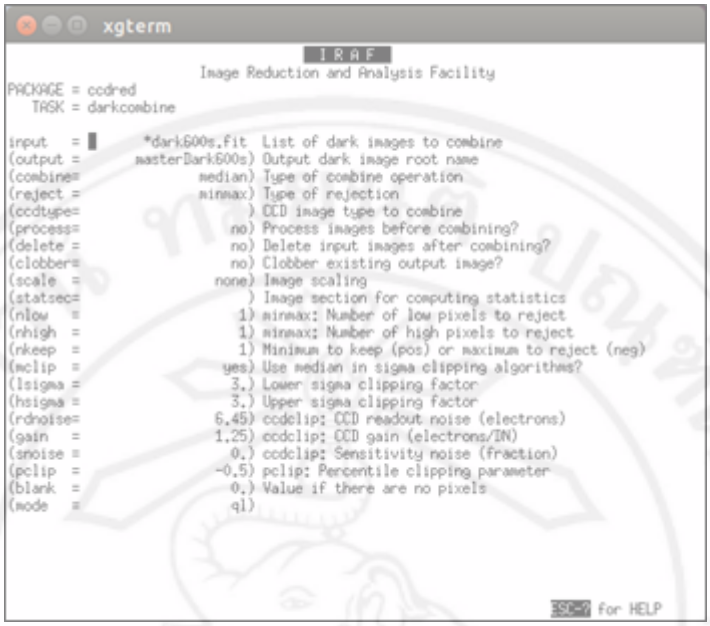

Figure 3.2: The parameters used in the "darkcombine" task to obtain the master dark frame using the median operation, no image scaling, 6.45 e^- CCD readout noise and 1.25 e^-/ ADU gain.

3.2.2 Flat Frame Combination

A flat frame is an image exposed to an evenly illuminated surface, such as twilight/ dawn sky or calibration lamp. A flat frame is used to fix a non-uniform image that is caused by optical instruments, such as dust on mirrors/filter surface and distortions along the optical path. To obtain the flat frame, the telescope is pointed to the sky at dawn and 11 images of the flat frame were captured for each filters (B, V, R_C, [SII], Red-continuum). The intensity of the flat images should be around half of the maximum pixel value or 20000 – 40000 count/pixel.

To combine the flat frames to a master flat, the "flatcombine" task in IRAF was used. The parameters used are shown in Figure 3.5, and a comparison of the flat frame and the master flat frame is in Figure 3.6.

Figure 3.3: One of the 11 dark frame images (left) before using “darkcombine” and the master dark frame (right) after using “darkcombine”. The images are compared with the same cut level.

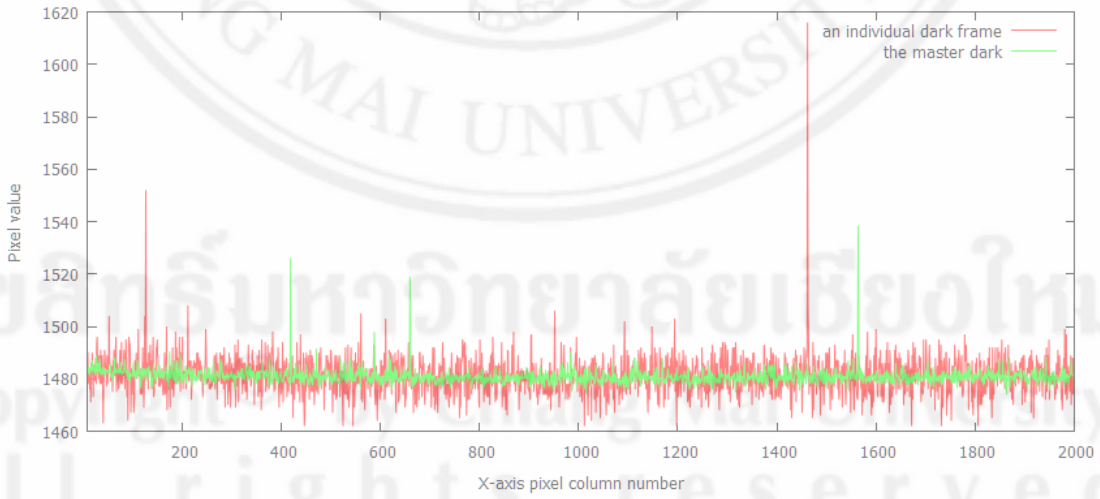

Figure 3.4: The count distribution of an individual dark frame (red) and the master dark (green) along the x-axis.

Figure 3.5: The parameters used in "flatcombine" task to obtain master flat frame in each filter using the median operation, no image scaling, 6.45 e^- CCD readout noise and 1.25 e^-/ADU gain.

Figure 3.6: One of the 11 flat frame image (R filter) before using "flatcombine" (left) and the image of the master flat frame after using "flatcombine" (right). The master flat frame has more signal and smoother than the left.

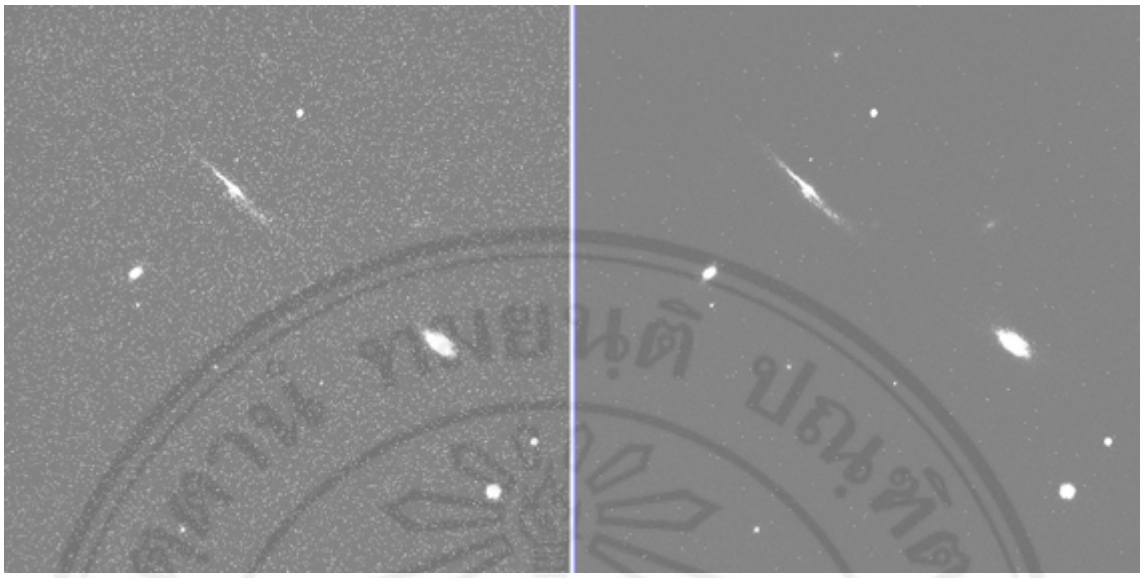

Figure 3.7: The raw scientific imaging data before applying the image reduction process (left) along with cleaned image (right) shown in power scale with the same cutting level.

3.2.3 Applying the Flat and Dark Frame to the Scientific Frame

We already have the essential material to make a scientific image reduction. We then apply the standard image reduction procedure that is described in Eq. 3.2 to obtain a cleaned image.

$$reduced\ image = \frac{raw\ scientific\ image - master\ dark\ frame}{normalized\ master\ flat frame} \tag{3.2}$$

.

The comparison of the raw image and cleaned image shown in figure 3.7.

3.3 Image Photometry

Photometry is about the measurement of light to determine the magnitude of celestial objects. In optical astronomy, the measurement of scientific data can be achieved by photometry. In our study, the first step after cleaning the imaging data is to use the photometric method called "Aperture Photometry" in GAIA to obtain a relative magnitude or instrument magnitude (m_i) of our object in each filter. The instrument magnitude

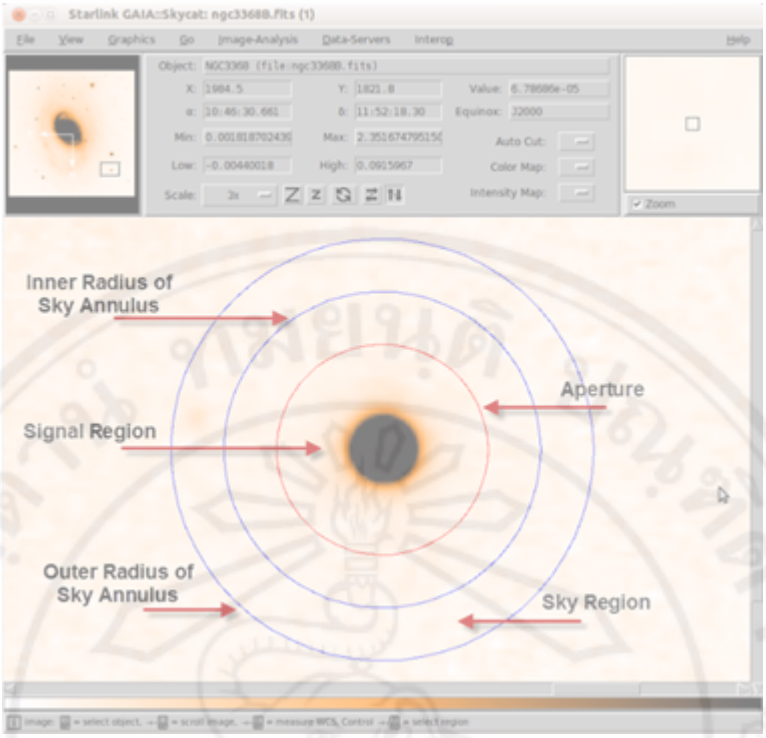

Figure 3.8: The aperture photometry GUI from GAIA astronomical tool.

is calculated using Eq.3.3. To determine the instrument magnitude, the object aperture parameters such as the semi-major axis, eccentricity (for ellipses only), inner and outer annulus scale positioning over the wanted sky objects must be defined first. The method about finding these parameters will be described in Section 3.4.

Flux or signal count can be acquired by integrating the individual pixels within the signal region subtracted from the sky region (see figure 3.8).

$$m_i = -2.5 \log\left(\frac{\int f \, da}{\tau}\right) , \tag{3.3}$$

where

m_i is an instrument magnitude,

f is an individual pixel signal value, and

τ is an integration time.

Error from GAIA Aperture Photometry

The error of instrument magnitude, $\sigma(m_i)$, extracted by GAIA photometry is

$$\sigma^2(m_i) = \frac{1}{g}\sum_{i}^{N_A}\frac{(S_i - \overline{B})^2}{N_i} + (N_A + \frac{N_A^2}{N_B})\sigma_{B/pix}^2 \quad , \tag{3.4}$$

where

g is the CCD GAIN value in electron/pixel unit,

N_A is the number of pixels in source,

N_B is the number of pixels in background annulus,

N_i is the depth level of coverage at pixel index i,

S_i is the signal value in pixel i,

$\overline{B}$ is the estimated mean background per pixel in annulus, and

$\sigma_{B/pix}^2$ is the background sky variance.

3.3.1 Determining the Zero Point

Because the magnitude calculated from the aperture photometry is a "relative" magnitude, the zero point must first be determined to obtain a corrected magnitude of the sky object. In this study, the zero point is determined by using the magnitude of standard stars located in our image. Using the magnitude from previous all-sky survey called "The USNO-B1.0 Catalog", the zero point is determined.

The zero point varies in each filter. Calculation for each filter can be done by using Eq. 3.5.

$$m_{zp} = m_{std} - m_i \quad , \tag{3.5}$$

where

m_{zp} is the zero point magnitude, and

m_{std} is the magnitude of standard star in USNO catalogue.

Error of Zero Point

$$\sigma^2(ZP) = \sigma_{std}^2 + \sigma^2(m_i) \tag{3.6}$$

$$\sigma_{std} = \frac{1}{\sqrt{N}}\sqrt{\sum_i^N \frac{(m_i - \overline{m_i})^2}{N-1}} \tag{3.7}$$

where

N is the number of reference stars in the FoV.

In this study, reference stars from USNO B1 catalog which contain the B, V and R_C image photometry were used to compare with the magnitude of the stars appearing in our FoV.

Table 3.2: Zero point and σ(ZP) in each filter

Filter	Number of reference stars	m_{zp}	$\sigma(ZP)$
B	14	31.04	0.10
V	14	31.19	0.11
R_C	14	30.80	0.13

3.3.2 Filter Correction

There are plenty of filter systems used in astronomy research. Each of them is designed to work for different purposes, characterized by the throughput of wavelength and bandpass (see Figure 3.6). To compare the imaging data across the filter systems, magnitude correction to reduce the uncertainty due to the different bandpass must be done.

To correct the magnitude, the area of the filter throughput was integrated in each filter. Then, the magnitude difference is obtained using the following Eq.

$$\triangle m = -2.5log(\frac{area\ of\ filter\ A}{area\ of\ filter\ B}) \quad , \tag{3.8}$$

where

$\triangle m$ is the magnitude difference.

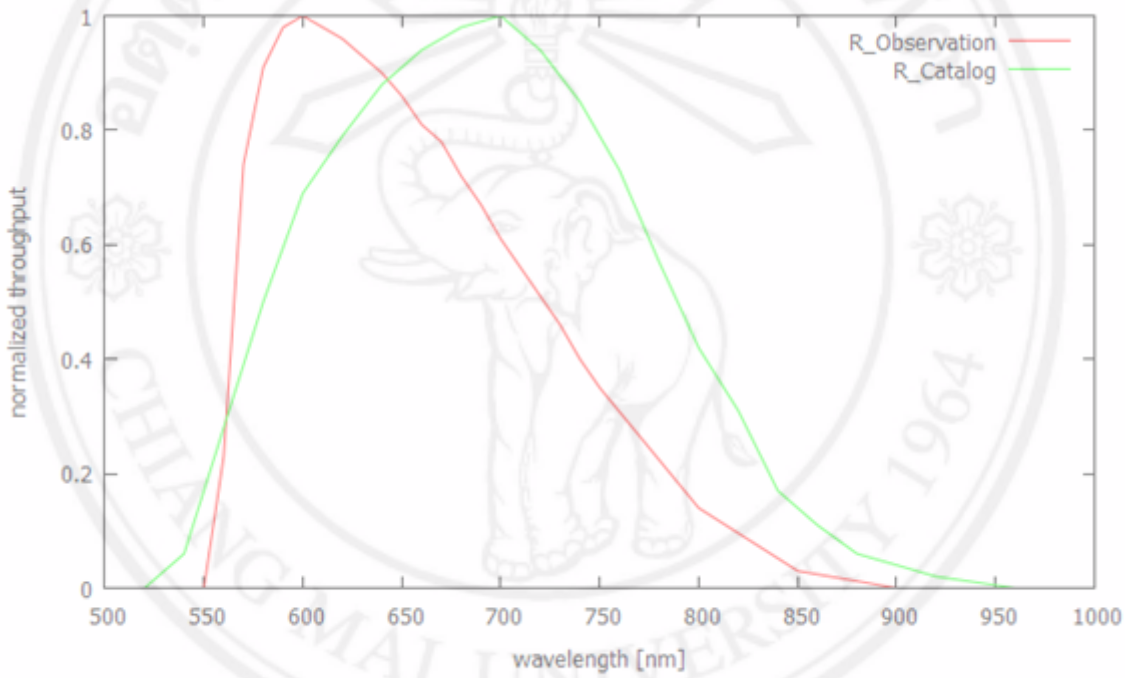

Figure 3.9: Comparison of the normalized throughput between the observation filter (green) and the catalog filter (red). The filter from the catalog can receive more light than the observation filter due to the wider bandpass, which is approximately 0.33 magnitude.

Using the corrected zero point and the magnitude difference, the corrected magnitude from the imaging data can then be determined using Eq. 3.9. After this section, I shall call R_C as R.

$$m_{corr} = m_i + m_{zp} \pm \triangle m \quad , \tag{3.9}$$

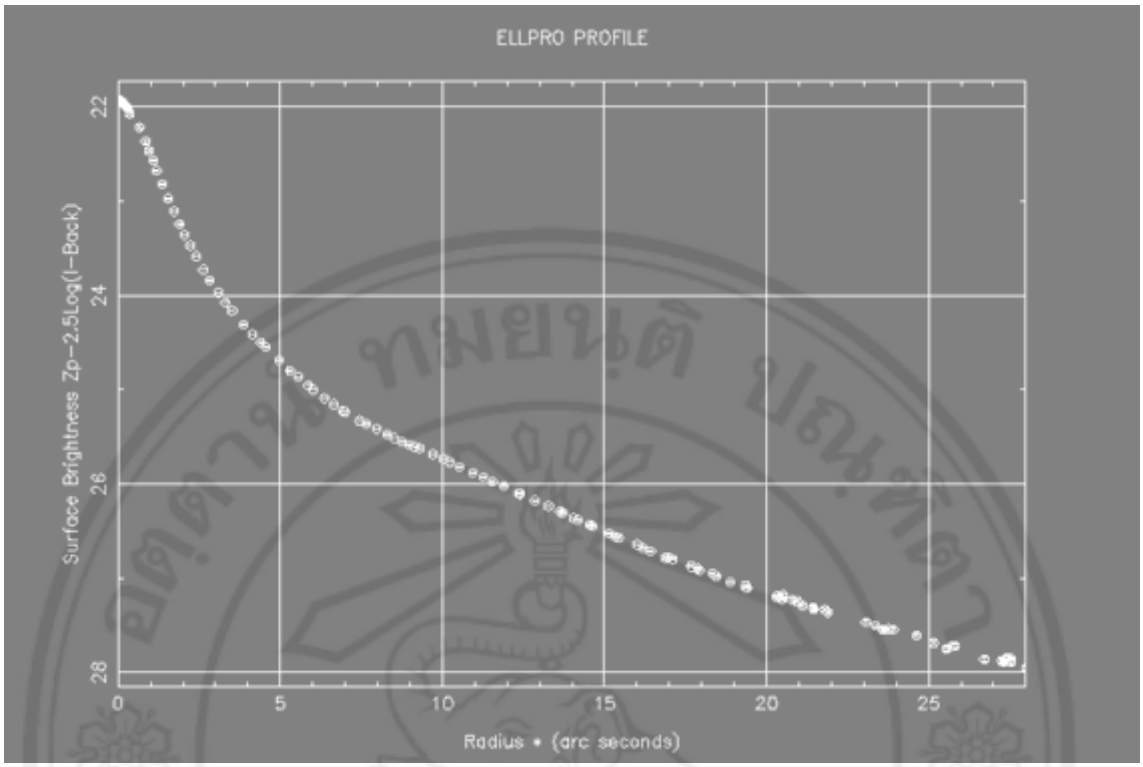

Figure 3.10: The brightness profile of NGC 4070, one of our sample galaxies. The "Radius" is the mean radius of the fitted ellipse or the square-root product of the semi-major and semi-minor axes that is equal to the ellipse area in arcsec.

where

m_{corr} is corrected magnitude.

3.3.3 Determining the Galaxy Diameter using B_{25}

Unlike stars, a galaxy is an extended surface object. To obtain the galaxy's magnitude, you must understand how large it is. In optical astronomy, one of the many ways to determine the boundary of the galaxy is to use the brightness profile. For this study, we applied the B_{25} method via ESP-ELLPRO from the GAIA astronomical tools to obtain the B_{25} isophote (see Figure 3.10). ESP-ELLPRO will create trial ellipses placed on the galaxy with different shapes and positions based on the surface brightness around the target. Then, we need to choose the ellipse that fits to the surface brightness at 25 magnitudes/arcsec^2 in B band.

Table 3.3: B, V and R instrument magnitude

No.	Name	$m_i(B)$	$m_i(V)$	$m_i(R)$
1	NGC 4070	14.10	13.21	12.90
2	J12040831+2023280	17.05	16.17	15.89
3	NGC 4066	14.10	13.22	12.94
4	NGC 4069	16.97	16.01	15.60
5	NGC 4060	16.00	15.17	14.93
6	NGC 4056	17.20	16.34	15.97
7	NGC 4065	14.55	13.60	13.20
8	J12040495+2014489	17.20	16.26	15.84
9	NGC 4061 (4055)	14.71	13.74	13.31
10	NGC 4072	16.31	15.32	14.92
11	UGC 07049	16.56	15.77	15.43
12	J12041217+2010251	17.79	16.82	16.46
13	NRGb177.059	19.12	18.21	17.72
14	J12043987+2013411	16.89	15.93	15.47
15	NGC 4076	14.79	14.11	13.73
16	J120425.68+201548.9	18.64	17.80	17.54
17	12042275+2015271	17.72	16.81	16.52
18	J12035600+2025499	17.05	16.07	15.66
19	J12034825+2024589	17.09	16.44	16.16
20	J12035132+2003099	16.17	15.40	15.24
21	J12032530+2014294	16.65	15.91	15.71

3.4 Hydrogen Alpha Equivalent Width

There are numerous tracers to track the star formation rate (SFR) in galaxies. In our study, we used the Hα emission line. This method was confirmed as a good tracer for observing star-formation rate in a normal disk galaxy (Kennicutt., 1983). To obtain the Hα emission line, we used the [SII] and Red-continuum narrowband filters, then calculated the Hα equivalent width to compare the star formation rate in each galaxy.

3.4.1 Continuum Ratio (CR)

In an optical observation, the flux counts cannot be directly obtained from the [SII] narrowband filter because it is already a combination of the flux counts of the Hα emission line and the continuum background flux, thus, we need to determine the ratio of these flux

counts and subtract the continuum background flux from the Hα emission line flux. We call this the Continuum Ratio (CR) [Kriwattanawong et al., 2011] and is calculated using Eq. 3.10

$$CR = \frac{count\ H\alpha}{count\ RedCon} \tag{3.10}$$

where

$count\ H\alpha$ is the flux count of the standard stars in SII image, and

$count\ RedCon$ is the flux count of the standard stars in Red-continuum image.

To use this equation, each standard star should not be a variable star and is assumed that it does not produce the Hα emission line. Then, we calculate the average of the CR in each image frame and apply it to the galaxy flux counts in the Red-continuum band.

Error of Flux Counts in Each Filter

$$\sigma(C_x) = \sqrt{\frac{C_x}{k_x}}\ , \tag{3.11}$$

where

k_x is the amount of photo-electrons per ADU in filter x.

Error of Continuum Ratio ($\sigma(CR)$)

$$\sigma(CR) = \frac{STD(CR)}{\sqrt{N}}\ , \tag{3.12}$$

where

$STD(CR)$ is the standard deviation of CR value, and

N is the number of sample.

Error of Continuum Flux Counts $\sigma(C_C)$

$$(\frac{\sigma(C_C)}{C_C})^2 = (\frac{\sigma(CR)}{CR})^2 + (\frac{\sigma(C_{RedCon})}{C_{RedCon}})^2 \tag{3.13}$$

where

C_C is the flux counts of continuum ($C_{RedCon} \times CR$)

3.4.2 Hα Flux count

After getting the CR of each scientific frame, the continuum flux count is subtracted from the [SII] scientific frame to obtain the pure Hα flux count using Eq. 3.14

$$C_{H\alpha} = C_{[SII]} - (C_{RedCon} \times CR) \tag{3.14}$$

where

$C_{H\alpha}$ is the subtracted flux counts of Hα.

This procedure will remove the continuum background flux out of the [SII] scientific frame. What remains is only the Hα flux count that we will use to calculate the EW(Hα).

Error of Hα flux count

$$\sigma(C_{H\alpha})^2 = \sigma(C_{[SII]})^2 + \sigma(C_C)^2 \tag{3.15}$$

3.4.3 The calculation of Hα Equivalent Width (EW(Hα))

Many quantities in astrophysics always come up with the equivalent width when it needs to compare properties in terms of wavelength, such as the Hα emission line which indicates the star formation rate activities in the galaxies. The calculation of EW(Hα) can be done by using Eq. 3.16 [Kriwattanawong et al., 2011].

Table 3.4: The CR values and its errors for each pointing

No.	Pointing	Name	C_{RedCon}	$\sigma(C_{RedCon})$	$C_{[SII]}$	$\sigma(C_{[SII]})$	CR	$\sigma(CR)$	$C_{H\alpha}$	$\sigma(C_{H\alpha})$
1	1	NGC 4070	2.93E+06	4.00E+04	3.03E+06	1.56E+03	9.33E-01	1.27E-02	1.04E+05	4.00E+04
2		J12040831+2023280	1.49E+05	2.06E+03	1.49E+05	3.46E+02			-1.07E+02	2.09E+03
3	2	NGC 4066	2.77E+06	7.79E+04	2.95E+06	1.54E+03	9.05E-01	2.55E-02	1.84E+05	7.79E+04
4	3	NGC 4069	2.44E+05	6.73E+03	2.66E+05	4.63E+02	1.05E+00	2.89E-02	2.18E+04	6.75E+03
5		NGC 4060	5.37E+05	1.48E+04	6.01E+05	6.96E+02			6.49E+04	1.48E+04
6		NGC 4056	1.87E+05	5.14E+03	1.85E+05	3.86E+02			-1.35E+03	5.16E+03
7	4	NGC 4065	2.69E+06	4.75E+04	2.80E+06	1.50E+03	9.42E-01	1.67E-02	1.15E+05	4.76E+04
8		J12040495+2014489	2.33E+05	4.14E+03	2.38E+05	4.38E+02			5.63E+03	4.16E+03
9		NGC 4061 (4055)	2.35E+06	4.16E+04	2.48E+06	1.41E+03			1.27E+05	4.16E+04
10	5	NGC 4072	6.26E+05	8.74E+03	6.64E+05	7.32E+02	9.85E-01	1.37E-02	3.84E+04	8.77E+03
11		UGC 07049	3.90E+05	5.46E+03	4.92E+05	6.30E+02			1.02E+05	5.49E+03
12		J12041217+2010251	1.45E+05	2.05E+03	1.46E+05	3.43E+02			4.69E+02	2.08E+03
13	6	NRGb177.059	5.13E+04	3.33E+02	5.85E+04	2.17E+02	9.94E-01	5.13E-03	7.25E+03	3.98E+02
14		J12043987+2013411	4.00E+05	2.14E+03	4.09E+05	5.75E+02			9.32E+03	2.22E+03
15		NGC 4076	2.06E+06	1.07E+04	2.27E+06	1.35E+03			2.05E+05	1.08E+04
16	7	J120425.68+201548.9	6.90E+04	2.06E+03	6.46E+04	2.28E+02	9.77E-01	2.89E-02	-4.45E+03	2.07E+03
17		12042275+2015271	1.62E+05	4.81E+03	1.63E+05	3.62E+02			7.51E+02	4.82E+03
18	8	J12035600+2025499	3.39E+05	1.84E+03	3.49E+05	5.31E+02	9.47E-01	4.93E-03	1.02E+04	1.91E+03
19		J12034825+2024589	2.37E+05	1.31E+03	2.60E+05	4.58E+02			2.24E+04	1.39E+03
20	9	J12035132+2003099	3.39E+05	8.45E+03	3.81E+05	5.54E+02	9.58E-01	2.38E-02	4.18E+04	8.47E+03
21	10	J12032530+2014294	1.85E+05	2.85E+03	1.98E+05	4.00E+02	9.20E-01	1.41E-02	1.33E+04	2.88E+03

$$EW(H\alpha) = \frac{\int T_n(\lambda)d\lambda}{T_n(6563+z)} \times \frac{C_{H\alpha}}{C_C} \quad , \tag{3.16}$$

where

T_n is the throughput of [SII] narrowband filter,

z is the redshift.

The narrowband of [SII] filter is shown in Fig. 3.11.

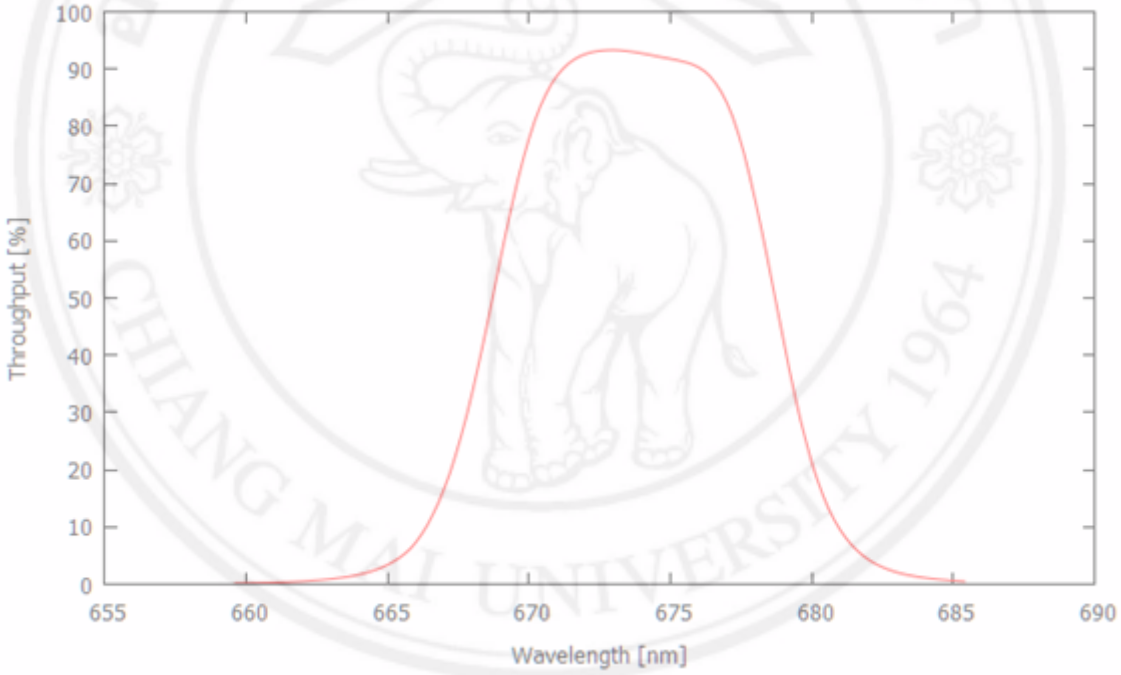

Figure 3.11: Transmissivity of [SII] narrowband filter.

Signal to Noise Ratio (S/N)

Signal to noise ratio tells us how much of the signal flux counts comes over the amount of noise and this can be calculated using Eq. 3.17, counting only the galaxy that has S/N $>$ 3.

$$S/N = \frac{C_{H\alpha}}{\sigma(C_{H\alpha})} \tag{3.17}$$

Error of EW(Hα)

$$\sigma(EW(H\alpha)) = \frac{EW(H\alpha)}{S/N} \tag{3.18}$$

3.5 Galaxy Morphological Classification

The galaxy morphological classification is another parameter that makes us understand the shape of the galaxy and classify them along the Hubble sequence and De Vaucouleurs system (Fig. 3.12) converted into *T-Type*, which is a number based from -6 to 10 (refer to Table 3.5).

The sample is divided into two groups, late-type galaxy (LTG) and early type galaxy (ETG) along the evolution sequence. Early type galaxy is the galaxy that has the *T-Type* number above zero and is shaped as a spiral. Late type galaxy is the elliptical galaxy with *T-Type* number below or equal zero.

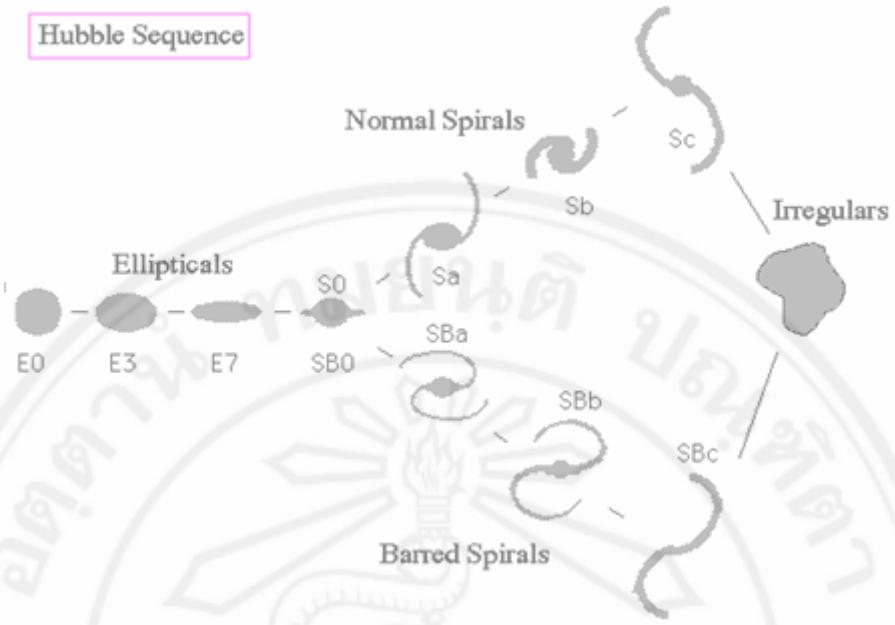

Figure 3.12: The galaxy classification along the Hubble sequence. (Source:*http:// abyss.uoregon.edu/ js/images/hubblefork.gif*).

Table 3.5: The Hubble sequence, De Vaucouleurs system and their equivalent *T-Type* number

Hubble sequence	De Vaucouleurs system	*T-Type*
	cE	-6
E	E	-5
	E^+	-4
	$S0^-$	-3
S0	S0	-2
	$S0^+$	-1
S0/a	S0/a	0
Sa	Sa	1
Sa-b	Sab	2
Sb	Sb	3
Sb-c	Sbc	4
	Sc	5
Sc	Scd	6
	Sd	7
Sc-Irr	Sdm	8
Irr	Sm	9
	Lm	10